SAF for Land Surface Analysis (LSA SAF)

Algorithm Theoretical Basis Document

Meteosat Second Generation Evapotranspiration (MET) Product Daily MET (DMET) Product

Reference Number: SAF/LAND/IM/ATBD_MET/1.2

Issue/Revision Index: Issue 1.2

Last Change: 11/03/2010

DOCUMENT SIGNATURE TABLE

	Name	Date	Signature
Prepared by:	RMI Team	11/03/2010	
Approved by:	Land SAF Project Manager (IM)		

DOCUMENTATION CHANGE RECORD

Issue / Revision	Date	Description:
Version 1.0	11/04/2008	Version presented to ORR3-ET (14 May 2008)
Version 1.1	10/07/2008	Version (1.0) including improprement after ORR3-ET
Version 1.2	11/03/2010	Version (1.1) including description of DMET calculation; presented to ORR (14 April 2010)

DISTRIBUTION LIST

Internal Consortium Distribution		
Organisation	**Name**	**No. Copies**
IM	Pedro Viterbo	
IM	Luís Pessanha	
IM	Isabel Trigo	
IDL	Carlos da Camara	
IM	Isabel Monteiro	
IM	Sandra Coelho	
IM	Carla Barroso	
IM	Pedro Diegues	
IM	Teresa Calado	
IM	Benvinda Barbosa	
IM	Ana Veloso	
IMK	Folke-S. Olesen	
IMK	Frank Goettsche	
IMK	Ewa Kabsch	
MF	Jean-Louis Roujean	
MF	Olivier Hautecoeur	
MF	Dominique Carrer	
RMI	Françoise Meulenberghs	
RMI	Arboleda Alirio	
RMI	Nicolas Ghilain	
FMI	Niilo Siljamo	
UV	Joaquin Melia	
UV	F. Javier García Haro	
UV/EOLAB	Fernando Camacho	
UV	Aleixander Verger	

External Distribution		
Organisation	**Name**	**No. Copies**
EUMETSAT	Frédéric Gasiglia	
EUMETSAT	Dominique Faucher	
EUMETSAT	Lorenzo Sarlo	
EUMETSAT	Lothar Schueller	
EDISOFT	Teresa Cardoso	
EDISOFT	Carlos Vicente	
EDISOFT	Cleber Balan	
SKYSOFT	Rui Alves	

SKYSOFT	João Canário	

Steering Group Distribution		
Nominated by:	**Name**	**No. Copies**
IM	Carlos Direitinho Tavares	
EUMETSAT	Lorenzo Sarlo	
EUMETSAT	Yves Govaerts	
EUMETSAT	François Montagner	
STG/AFG (UGM)	Luigi de Leonibus	
MF	François Bouyssel	
RMI	Alexandre Joukoff	
FMI	Tapio Tuomi	

TABLE OF CONTENTS

1   Introduction

The evapotranspiration (ET) algorithm developed in the framework of LSA-SAF targets the quantification of the flux of water vapour releases from the ground surface (soil and canopy) into the atmosphere using input data derived from MSG satellites. The 'MET' acronym is used for 'MSG ET'. Present document aims to describe in detail the methodology adopted for the version 04 of the LSA-SAF ET algorithm. Two other documents are available. The 'validation report' (VR) gathers all results of performed validation tests. The 'product user manual' (PUM) provides a detailed description of the model output (product characteristics, file format and content structure).

Satellite remote sensing (SRS) stays as the only method capable of providing wide area coverage of environmental variables at economically affordable costs. However, a major difficulty to the use of SRS for monitoring ET at regional and global scale is that the phase change of water molecules produces neither emission nor absorption of an electromagnetic signal. Therefore, ET process is not directly quantifiable from satellite observations. It has to be assessed, taking advantage of information gained through the satellite about surface variables influencing evapotranspiration (Choudhury, 1991). Most of proposed methods use SRS derived data combined into models with different degrees of complexity ranging from empirical direct methods to complex deterministic models based on SVAT modules that compute the different components of the energy budget (see e.g. Courault et al. (2005), for a short review). Simplest methods are only applicable locally, where they were calibrated. Most methods can only be applied for clear sky conditions. This is the case for methods requiring as input Land Surface Temperature (LST). Furthermore, zenital angle restrictions can limit the availability of LST like in the case of LSA-SAF LST product.

The methodological approaches selected in the framework of the LSA-SAF intends to be applicable at regional to global scales, to be able to provide a monitoring at short time step to follow the diurnal cycle evolution and to obtain results continuously for all nebulosity conditions. Due to its limited availability LST is not exploited in the current version of the algorithm. However, a possible use as ancillary data will be investigated in the future. The adopted method can be described as a SVAT scheme modified to accept input data from external sources (Gellens-Meulenberghs et al., 2006, 2007). It is based on the physics of the Tiled ECMWF Surface Scheme for Exchange Processes over Land, TESSEL (Viterbo and Beljaars, 1995; van den Hurk et al., 2000). Main modifications operated to the initial model allow the model to run decoupled from the atmospheric model and to use data from external sources like SRS derived data, NWP output and recent information about land-cover characteristics. In this approach, the area for which ET has to be assessed is divided into independent pixels, in a one-to-one correspondence with the pixels of a satellite image. Each pixel is in turn considered as being a mix of homogeneous *tiles*, each tile representing a particular soil surface: bare soil, short canopy, high canopy, *etc*. The global pixel value is obtained through the weighted contribution of each tile. Theoretically, ET can be derived in

near real time at the time resolution of MSG satellite images. In practice, the generation of ET will be limited by the availability of input data. Since radiation components from LSA-SAF are generated every 30 minutes, LSA-SAF MET is produced at the same frequency.

The next section describes the methodology. It is dedicated to the detailed description of the model used: physical equations, parameterisation and assumptions. The third section deals with the input variables used in the context of the LSA-SAF. A sensitivity analysis of the method is presented in a fourth section. A fifth section presents a short description of the model output. The adopted methodology combines the forces of remote sensing approaches and NWP models. Expert knowledge about the global ET product quality and its added value is provided in a final section.

2   Methodology

The elementary spatial unit of the model is called *pixel* in reference to the basic unit of the SEVIRI instrument on board of MSG satellites. The dimension of the surface represented by a pixel varies in function of its location (longitude and latitude) and is 3x3 km at MSG sub satellite point. The size of a pixel over the European region is about 4x5 km. Since the vegetation cover influences most of the surface atmospheric processes over land, the estimation of ET is made by reference to a land cover map which provides the fraction of vegetation types within each MSG pixel. The different vegetation types considered in the MET algorithm are listed in Table 1. This primary vegetation types are called "tiles" and each pixel may be composed of several tiles. In practice, a maximum of four tiles (3 vegetation tiles + bare soil) are allowed by pixel. ET is calculated separately for each tile in pixel and the pixel value is obtained by a weighted contribution of all tiles composing the pixel.

#	Vegetation type	$r_{s,min}$ [s/m]	g_D [hPa^{-1}]
1	Bare soil	50	0
2	Snow	NA	NA
3	Deciduous Broadleaved trees	300	0.03
4	Evergreen Needleleaved trees	250	0.03
5	Evergreen Broadleaved trees	250	0.03
6	Crops	180	0
7	Irrigated crops	180	0
8	Grass	110	0
9	Bogs and Marshes	250	0

Table 1 Vegetation type considered by MET algorithm and associated parameters rs_min (minimum stomatal resistance) and g_D (coefficient for the dependency of canopy resistance –rc- on water vapour pressure deficit)

2.1 Model description at tile level

The surface energy balance is computed by the algorithm at tile level in a conceptual layer, called *skin* layer. This latter represents the coverage of the land surface (vegetation, bare soil, snow) as a flat layer, without description of the 3-D structure of the canopy.

The MET algorithm is an energy balance model aiming to compute, for each tile i in the considered pixel, the partition of net radiation (R_{ni}), sensible heat flux (H_i), latent heat flux (LE_i) and heat conduction flux into the ground (G_i) according to

$$R_{ni} - H_i - LE_i - G_i = 0 \tag{1}$$

In this relationship the following sign convention is adopted: R_{ni} is positive downward whereas the three other fluxes are positive upward. In this way, all the fluxes are positive during daytime and can be easily compared and represented graphically.

The land cover influences the repartition of the surface fluxes and the forcing fields used in the model. The main input data are solar radiation at surface ($S_\downarrow$), long-wave radiation at surface ($L_\downarrow$), air temperature (T_a) and specific humidity (q_a) at reference height (z_a), surface air pressure (P_a), wind speed (U_a) at reference height (z), surface albedo (α), soil temperature (T_k) and soil moisture (θ_k) at four soil depths (k).

2.1.1 Net radiation

The net radiation is given by

$$R_n = (1-\alpha)S_\downarrow + \varepsilon(L_\downarrow - \sigma T_{sk,i}^4) \tag{2}$$

where ε is the surface emissivity, $T_{sk,i}$ is the skin temperature (K), σ is the Stephan-Boltzmann constant (5.67 10^{-8} W m^{-2} K^{-4}).

2.1.2 Heat flux conduction into the ground

A common choice to parameterize the soil heat flux (G_i) is to approximate it as a fraction (β_i) of the net surface radiation ($R_{n_{i}}$), assuming that it has a diurnal variation in phase with the net radiation following

$$G_i = \beta_i . R_{n_i} \tag{3}$$

8

While different variants based on the same assumption exist in the literature (Choudury et al., 1987; Bastiaansen, 1995; Norman et al., 1995; Jacobsen and Hansen, 1999; Friedl, 2002; Kustas et al., 1993; Santanello and Friedl, 2003), we choose the parameterization of Chebhouni et al. (1996). This parameterisation requires only the knowledge of Leaf Area Index (*LAI*). The heat conduction flux into the soil is calculated according to equation 3. In this equation, coefficient β_i is calculated as a function of LAI via the Modified Soil Adjusted Vegetation Index (MSAVI)

$$\beta_i = 0.5.\exp(a_1.MSAVI_i) \qquad \text{where } a_1 = -2.13 \qquad (4)$$

$$MSAVI_i = a_2 - a_3.\exp(-a_4.LAI_i) \qquad \text{where } a_2 = 0.88, \ a_3 = 0.78, \ a_4 = 0.6 \qquad (5)$$

Leaf area index used in the model are generated from the monthly ECOCLIMAP LAI fields at tile level. The figure 1 shows the ECOCLIMAP leaf area index for the dominant tile over Europe for the month of May, the MSAVI image (calculated with equation 5) and the β_i image (calculated with equation 4) for Europe.
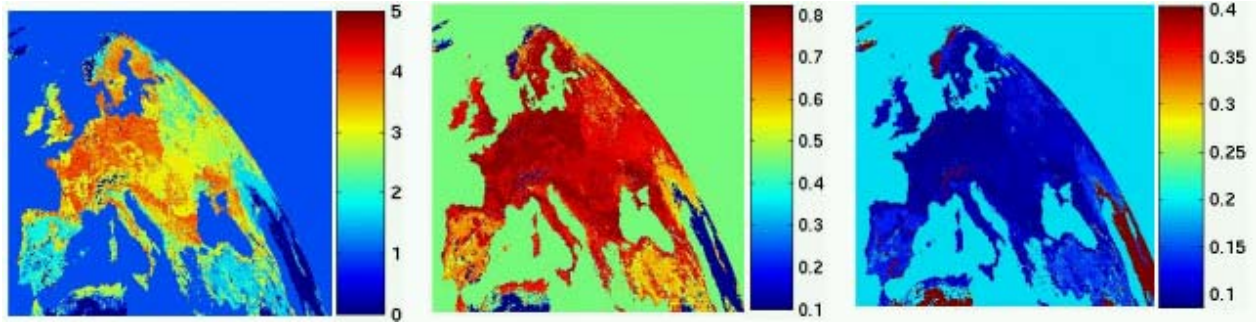
Figure 1, Beta (β_i, right) and MSAVI(center) images generated from the ECOCLIMAP LAI (left) for the dominant tile over Europe, for the month of May.

2.1.3 Latent and sensible heat fluxes

The latent and sensible heat fluxes are obtained via a resistance approach according to equations 6 and 7 respectively.

$$LE_i = \frac{L_v \rho_a}{\left(r_{a_i} + r_{c_i}\right)}\left[q_{sat}\left(T_{sk,i}\right) - q_a\left(T_a\right)\right] \qquad (6)$$

$$H_i = \frac{\rho_a}{r_{a_i}}\left[c_p(T_{sk,i} - T_a) - gz_a\right] \qquad (7)$$

In this equation ρ_a is the air density, r_a the aerodynamic resistance, z_a is the reference height above the surface that corresponds to the given air temperature and humidity, z is the height

corresponding to the wind speed, r_c is the canopy resistance, q_a the specific humidity, q_{sat} the specific humidity at saturation.

The aerodynamic resistance ($r_{a_{i_i}}$) is directly connected to the stability of the atmosphere, as shown in equation 8. Friction velocity ($u_{*_{i}}$) and Obukhov length (L_i) are therefore needed to calculate the aerodynamic resistance and are expressed in equations 9 and 10 respectively.

$$\frac{1}{r_{a_i}} = \frac{ku_{*_i}}{\ln\left(\frac{z_a - d_i}{z_{0hi}}\right) - \Psi_h\left(\frac{z_a - d_i}{L_i}\right) + \Psi_h\left(\frac{z_{0hi}}{L_i}\right)} \tag{8}$$

$$u_{*_i} = \frac{kU_a}{\ln\left(\frac{z - d_i}{z_{0m_i}}\right) - \Psi_m\left(\frac{z - d_i}{L_i}\right) + \Psi_m\left(\frac{z_{0mi}}{L_i}\right)} \tag{9}$$

$$L_i = \frac{\rho_a u_{*_i}^3}{kg\left(\frac{H_i}{c_p T_a} + 0.608\frac{LE_i}{L_v}\right)} \tag{10}$$

In this equations Ψ_h and Ψ_m are, respectively, the sensible heat and momentum stability functions, as described in Beljaars and Viterbo (1994). Sensible and latent heat fluxes are needed in equation 10 to compute the Obukhov length, the complete system of non-linear equations has to be solved iteratively (see section 2.3 for solving procedure)

The canopy resistance r_c used for vegetation is computed by adopting the Tessel formulation given by

$$r_c = \frac{r_{s,\min}}{LAI} f_1(S\!\downarrow)f_2(\bar{\theta})f_3(D_a) \tag{11}$$

as a function of incoming solar radiation at the surface ($S_\downarrow$), average unfrozen soil water content ($\bar{\theta}$), atmospheric water pressure deficit (D_a), leaf area index (*LAI*) and minimum stomatal resistance ($r_{s,min}$). The minimum stomatal resistance scaled by LAI fixes the maximum rate of evapotranspiration observed for each vegetation type in absence of any constrains. Values of $r_{s,min}$ are taken from ECOCLIMAP or recalibrated. The adopted values are listed in Table 1.

The Jarvis functions are given by:

$$f_1(S_\downarrow)^{-1} = \min\left(1, \frac{b.S_\downarrow + c}{a.(b.S_\downarrow + 1)}\right) \tag{12}$$

$$f_2(\overline{\theta})^{-1} = \frac{\overline{\theta} - \theta_{pwp}}{\theta_{cap} - \theta_{pwp}} \qquad \text{if } \theta_{pwp} \leq \overline{\theta} \leq \theta_{cap};$$

$$f_2(\overline{\theta})^{-1} = 0 \qquad \text{elsewhere} \tag{13}$$

$$f_3(D_a)^{-1} = \exp(-g_D.D_a) \tag{14}$$

with

$$D_a = e_{sat}(T_a) - e(T_a) \tag{15}$$

where e is the water vapour pressure.

Averaged soil water content in the root-zone, available for the transpiration of plants via function f_2, is computed by means of equation 16. The four-layered soil moisture is modulated by a function of soil temperature to take in account the phase of the water in the soil (equation 17) and is combined in a weighted average value, using the plants roots distribution in soil (Table 2).

$$\overline{\theta} = \sum_{k=1}^{4} R_k.\max(f_{liq,k}.\theta_k, \theta_{pwp}) \tag{16}$$

$$f_{liq,k} = \begin{cases} 1 & \text{if } T_k > T_{f1} \\ 1 - 0.5.\left\{1 - \sin\left[\frac{\pi.(T_k - 0.5.T_{f1} - 0.5.T_{f2})}{T_{f1} - T_{f2}}\right]\right\} & \text{if } T_{f2} \leq T_k \leq T_{f1} \\ 0 & \text{if } T_k \leq T_{f2} \end{cases} \tag{17}$$

with T_{f1} and T_{f2} being two constant temperatures of 1°C (274.15 °K) and –3 °C (270.15°K).

Vegetation type	1	2	3	4	5	6	7	8	9
Layer 1	100	-	24	26	25	24	24	35	25
Layer 2	0	-	38	39	34	41	41	38	34
Layer 3	0	-	31	29	27	31	31	23	27
Layer 4	0	-	7	6	14	4	4	4	11

Table 2 Roots distribution (R_k) per vegetation type (in %) over the four soil layers. Vegetation types are listed in Table 1.

A separate formulation is used for bare soil. In this case relationship (11) is not used and is replaced by (18). A minimum stomatal resistance is associated to bare soil (Table 1) to represent the minimum soil resistance and the only stress assumed for soil evaporation is due to soil water deficit, via the Jarvis function f_2.

$$r_c = r_{s,\min} . f_2(f_{liq}.\theta_1) \tag{18}$$

2.2 Averaging at pixel level

Heat flux values for the whole pixel are calculated as a weighted contribution of each tile

$$LE = \sum \zeta_i LE_i \qquad \text{and} \qquad H = \sum \zeta_i H_i \tag{19}$$

where ζ_i is the fraction of i tile in pixel.

Derivation of the evapotranspiration.

The LE obtained for the whole pixel is expressed in W/m². The corresponding evapotranspiration values, expressed in mm/h is given by

$$ET = 3600.LE / L_v \tag{20}$$

with the latent heat of vaporization (L_v) is given by

$$L_v = [2.501 \text{-} 0.00234 \, (T_a - 273.15)] \, 10^6 \tag{21}$$

Sublimation from snow is not considered.

2.3 Equation solving procedure

Solving the equations (1), (6), (7) and (9) taking relations (2), (3), (4), (5), (8) and (10) into account requires an iterative method, because of the non-linear inter-dependence of the variables *H, LE, T_{sk} and u_**. In the ET implementation, a single point iteration method has been selected for solving the system of equations, assuming neutral stability as initial condition. Iteration is stopped when pixel estimates of the four key-variables (*H, LE, T_{sk}, u_**) are stabilized, using a predefined precision (difference between two successive iteration less than 0.015 for H and LE) criterion. When the number of iterations exceeds 100, the process is stopped and algorithm returns the flag 'not-converged'.

2.4 Daily evapotranspiration product (DMET)

Daily evapotranspiration are obtained by temporal integration of instantaneous values generated by the MET algorithm according to

$$DMET = \int_{h_1}^{h_2} MET_i(t)dt \tag{22}$$

where MET_i are the instantaneous evapotranspiration estimated provided by the MET algorithm every 30 minutes for a given day. The integration limits ($h1$, $h2$) correspond to the first (theoretically at 00:30 UTC) and last (theoretically at 24:00 UTC) existing slots for a given day. In the best situation, a total of 48 images are generated by day what means that for each MSG pixel, 48 ET values have to be integrated. It happens that some images are missing for a given day. In order to provide a daily consistent value for each pixel, a linear interpolation between the closest slots is applied according to

$$MET_j = MET_{j-1} + 0.5\,(MET_j + MET_{j-1})\,N \tag{23}$$

where MET_{j-1} and MET_j are previous and next existing ET values for the same pixel in considered day and N is the number of time steps between previous and next existing ET values.

3 Input data

The main input data necessary to retrieve MET are solar radiation at surface ($S_\downarrow$), long-wave radiation at surface ($L_\downarrow$), air temperature (T_a) and specific humidity (q_a) at reference height (z_a), surface air pressure (P_a), wind speed (U_a) at reference height (z), surface albedo (α), soil temperature (T_k) and soil moisture (θ_k) at four soil depths (k). Input data can be divided into three categories: a) radiative forcing used for the computation of the net radiation available at surface; b) meteorological forcing (Numerical Weather Prediction data); and c) land-cover information. Radiative forcing is derived from SRS (through other LSA-SAF products), meteorological forcing is obtained from numerical weather prediction (NWP) models (ECMWF forecasts) and land-cover information is derived from the ECOCLIMAP land cover data base. More details and examples of input data are provided below.

Category	radiative data	meteorological data	land cover database
source	SRS	NWP	SRS
variability	dynamic	dynamic	semi-static

Table 3, categories of MET input data.

3.1 LSA-SAF data

Radiative variables driving the model are taken from corresponding LSA-SAF products. These variables are

- solar radiation at surface ($S_\downarrow$) provided by LSA-SAF Downward Surface Short-wave Flux (DSSF), figure 2.

- long-wave radiation at surface ($L_\downarrow$) provided by LSA-SAF Downward Surface Long-wave Flux (DSLF), figure 3 and

- albedo (α) provided by LSA-SAF albedo (AL), figure 4.

For situations where LSA-SAF AL is missing or its associated error is larger than 50%, the monthly albedo provided by the ECOCLIMAP database (figure 11) is used and the pixel quality flag is consequently degraded. The temporal sampling rates of these products are 15 minutes for DSSF, 30 minutes for DSLF and 1 day for AL. The spatial resolution of these products is the nominal resolution of the SEVIRI imager.
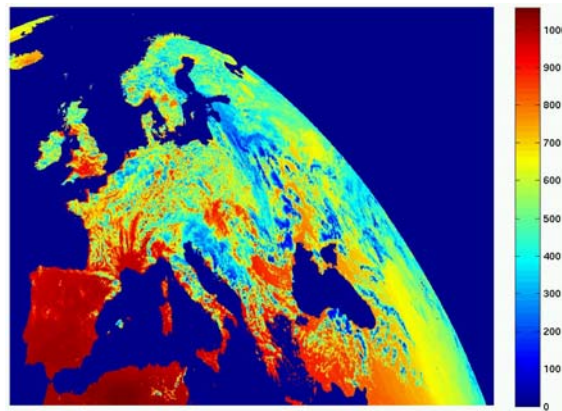

Figure 2, LSA-SAF DSSF (W m-^{2}) for 14th June 2008 at 12h UTC.
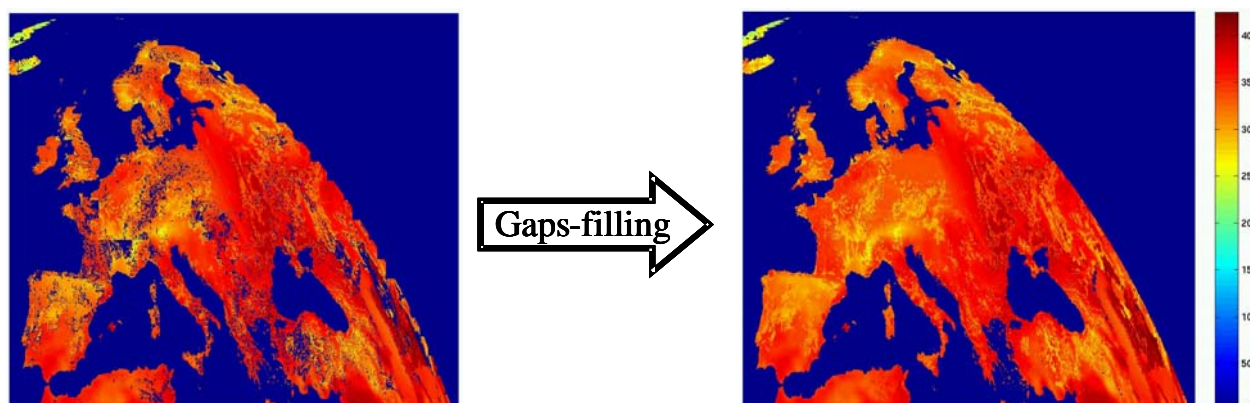
14

Figure 3, LSA-SAF DSLF product (W m^{-2}) for 14th June 2008 at 12h UTC. On the left the original product and on the right the product after applying the gaps filling procedure.
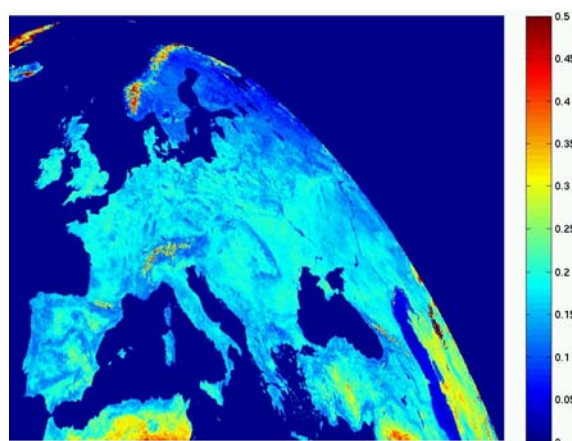
Figure 4, LSA-SAF Albedo (AL) product for 14th June 2008 at 12h UTC.

3.2   Numerical weather prediction data

Meteorological auxiliary data needed by the ET algorithm is retrieved from ECMWF forecasts. This data originally gathered at ECMWF spatial resolution, i.e. 0.25°x0.25°, is mapped into the MSG grid and spatially interpolated for air temperature (figure 5), dew point temperature (figure 6), 10-meters wind speed (figure 7), surface atmospheric pressure (figure 8), soil moisture and soil temperature in the 4 soil layers. These meteorological fields are also linearly interpolated from three hours to one hour. Dew point temperature, air temperature and air pressure are used to calculate air specific humidity used in equation 6. Soil moisture and soil temperature are used jointly to compute the liquid fraction of soil water content available for evapotranspiration in the root-zone and in the superficial soil layer. Figure 9 represents temperature and moisture from the upper soil layer.
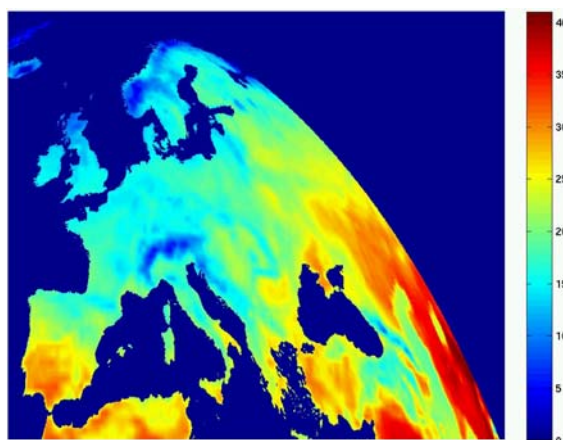
Figure 5, ECMWF 2m air temperature (C) for 14th June 2008 at 12h UTC.
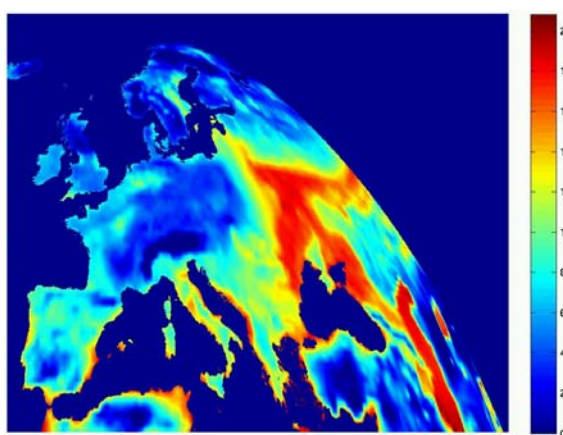
Figure 6, ECMWF dew-point temperature (C) for 14th June 2008 at 12h UTC.
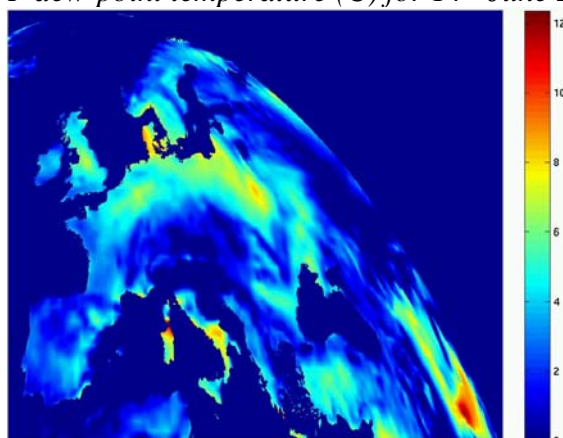
Figure 7, ECMWF wind speed (m s^{-1}) for 14th June 2008 at 12h UTC.

16
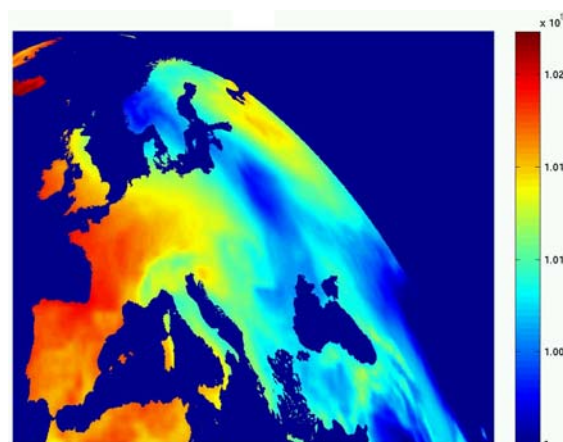
Figure 8, ECMWF surface atmospheric pressure (hPa) for 14th June 2008 at 12h UTC
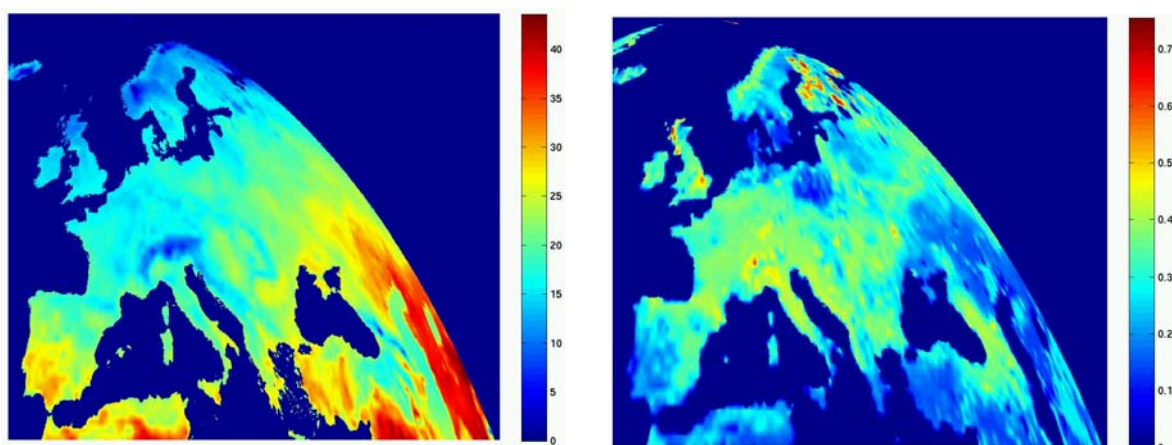
Figure 9, ECMWF first soil layer soil temperature (°C) (left) and soil moisture content (m³/m³) (right) for 14th June 2008 at 12h UTC.

Since November 2007, a new parameterization has been adopted at ECMWF for SM. Implication for usage as input into MET algorithm is described in Annex A.

3.3   Land cover data base

ECOCLIMAP is a surface parameter global database at a 1 km resolution developed by Meteo-France (Masson et al., 2003). It is well suited for use in SVAT schemes embedded in meteorological and climate models at all horizontal scales. It supports the tiling approach currently implemented in many well-known SVAT schemes. In this database tile parameters vary on monthly basis, depending on vegetation types and climatic regions.

17

The Evapotranspiration (ET) algorithm developed in the framework of the LSA-SAF is based on the tile approach, and surface parameters related to cover types are derived from the ECOCLIMAP database.

The following ECOCLIMAP fields are currently used:
- Vegetation cover
- Tiles distribution
- Leaf Area Index (LAI) on tile basis
- Roughness length on tile basis
- Minimum stomatal resistance on tile basis
- Surface Albedo (only when LSA-SAF AL is missing or is of bad quality).

The LSA-SAF ET algorithm uses a set of Tessel parameters available for 9 different land cover types. ECOCLIMAP gives a land-cover classification in terms of 11 elementary classes. These have been associated to the Tessel land cover types according to Table 4.

ECOCLIMAP	LSA-SAF MET algorithm
1. bare soil	1. bare soil
2. rocks	1. bare soil
3. permanent snow	2. snow
4. deciduous broadleaf trees	3. deciduous broadleaf trees
5. coniferous trees	4. evergreen needleleaf trees
6. evergreen broadleaf trees	5. evergreen broadleaf trees
7. C3 crops	6. crops, mixed farming
8. C4 crops	7. irrigated crops
9. irrigated crops	7. irrigated crops
10. natural herbaceous not irrigated	8. short grass
11. swamp herbaceous and gardens	9. bogs and marshes

Table 4, ECOCLIMAP tiles associated to LSA-SAF-ET model tiles.

In the MET approach, different tiles are allowed in each single pixel what is more realistic than the adoption of the dominant land cover type, particularly in very patchy landscapes. Figure 10 represents the first and second most representative tiles for each MSG pixel over Europe for the 11 ECOCLIMAP classes. Figure 11 shows the ECOCLIMAP albedo values for the month of June.
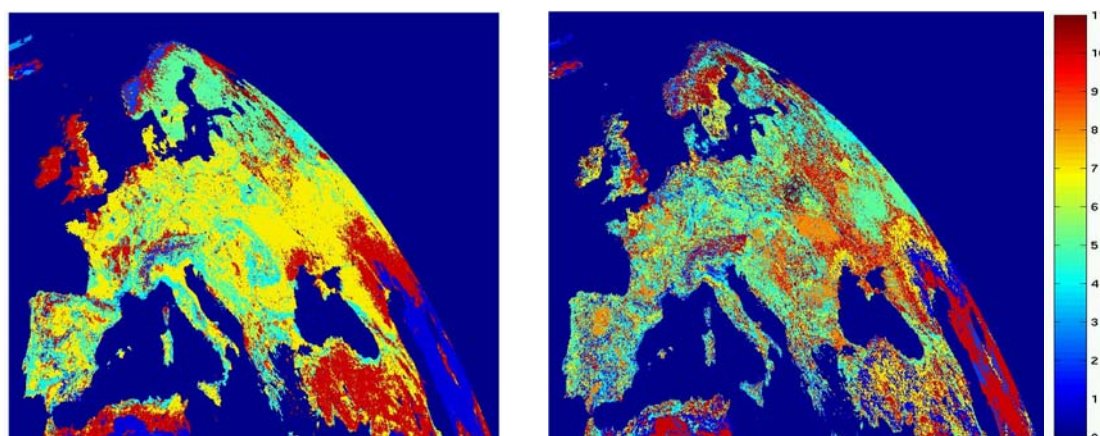
Figure 10, ECOCLIMAP first (left) and second (right) tiles over the MSG grid.
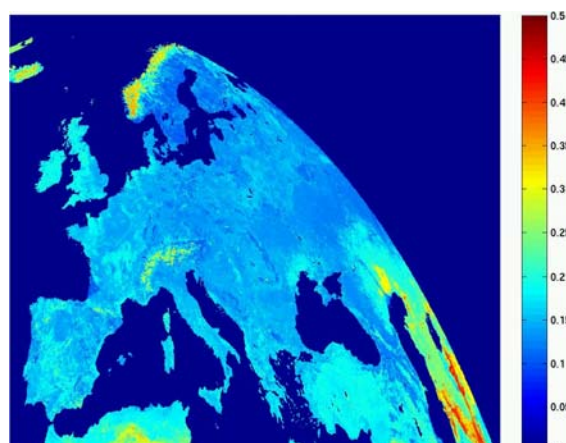
Figure 11, ECOCLIMAP albedo for the month of June, over the MSG grid.

4   Sensitivity Analysis

Main sources of uncertainties cumulated on the MET product deal with sensors performance, accuracy of cloudy pixels identification, accuracy of atmospheric corrections, surface heterogeneity and land cover classification. Those uncertainties influence directly or indirectly the performances of variable like DSSF, DSLF, and AL that in turn provide input for the MET algorithm. In order to evaluate the impact of input variables uncertainties on the performances of the MET algorithm, a sensibility analysis was performed over the main algorithm forcing.

4.1   Methodology

In order to evaluate the uncertainties of a determined input data, we consider a fluctuating error, chosen randomly into a unbiased Gaussian distribution with a standard deviation associated to the known products (or variables) error (for example, for DSLF, the RMSE is of 10% of the actual value). At each time step, the fluctuation term is re-evaluated randomly. A period of about 10 days is considered for these tests (the dataset of Cabauw for LSA-SAF products and FIFE for the other input variables). The MET algorithm is run 5000 times (or 15000 for global analysis) for each 30 minutes time step, to increase the statistics. With this amount of simulations, different from each other, we compute for each time step the standard deviation of the ET distribution produced. Eliminating night values and diverging ones, we make an estimation of the error induced by the input uncertainties by analyzing statistical properties of resulting distributions. A control simulation, consisting of a simple run with the given input data, is also carried out to check that no bias will be introduced in the results.

Datasets:
-Cabauw: 19-30 June 1995, mainly clear sky, input radiation from Cabauw dataset, meteorological variables from ERA40.
-FIFE: 19-30 June 1987, mainly clear sky, input radiation from FIFE dataset, meteorological variables from ERA40.

4.2   Results

Five sensitivity analyses have been performed, four concerning partial/individual sensitivity analyses and one impact analysis of the uncertainty of all input variables together (except soil moisture). Each of these 5 tests is summarized in Table *5*. For all these tests, it is found that uncertainty on ET induced by input variable uncertainty shows a diurnal cycle. The results obtained for tests 1 to 3 are presented in Figure 12. In this figure, relative error is displayed in function of the short-wave incoming radiation measured at surface, which is a good indicator of diurnal evolution during short clear sky periods. For wind speed, distributions of induced ET for test 4 are displayed in Figure 13.

Analysis	Variable	σ	Dataset
Individual Analysis 1	DSSF	15 W/m²	Cabauw
	DSLF	10% of the actual value	
	AL	10% of the actual value	
Individual Analysis 2	Specific air humidity	20% of the actual value	FIFE
Individual Analysis 3	Air temperature	2 K	FIFE
Individual Analysis 4	Wind speed	10% & 20% of the actual value	FIFE
Overall Analysis	DSSF	15 W/m²	FIFE
	DSLF	10% of the actual value	
	AL	10% of the actual value	
	Specific air humidity	20% of the actual value	
	Air temperature	2 K	
	Wind speed	10% of the actual value	

Table 5: Summary of the conditions on the 5 tests performed to assess the sensitivity of MET algorithm to uncertainty to input variables. The first four tests are designed to assess the sensitivity to individual input components and the last test is dedicated to evaluate the overall error on ET induced by uncertainty on all input variables. The table list for each test the variables to be tested, the associated error and the datasetused for each analysis.
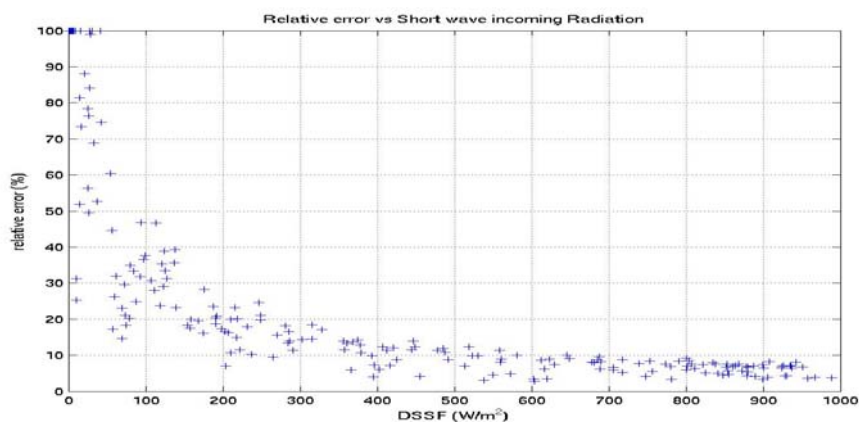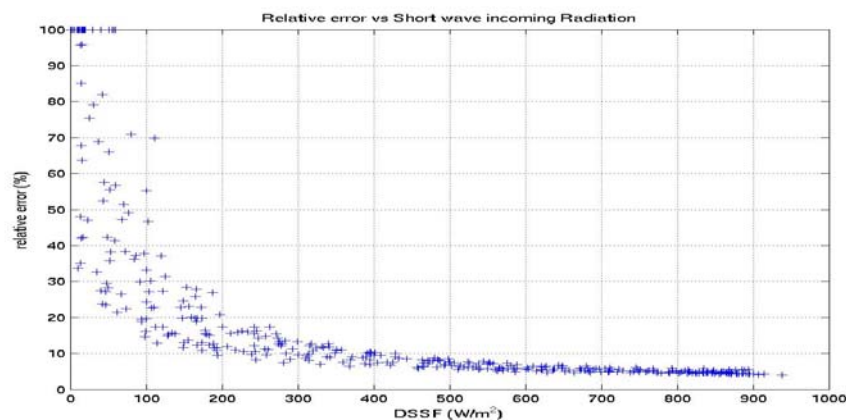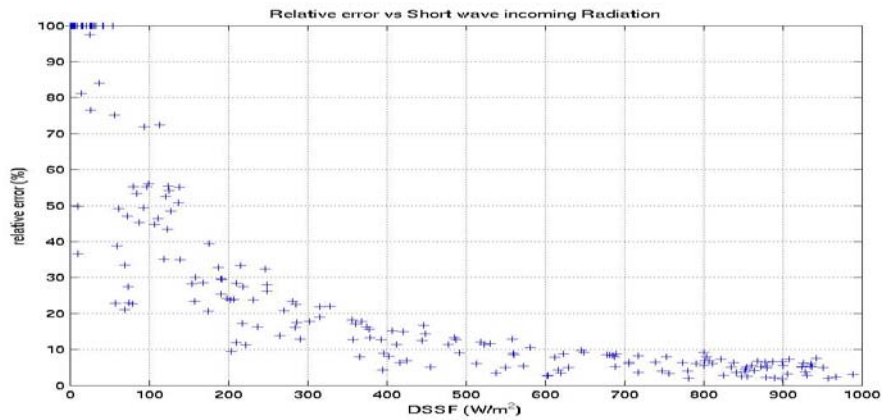
Figure 12: Relation between DSSF range and relative error estimated from individual analyses 1, 2 and 3. ET values computed for small DSSF are very sensitive to uncertainty on radiation variables.
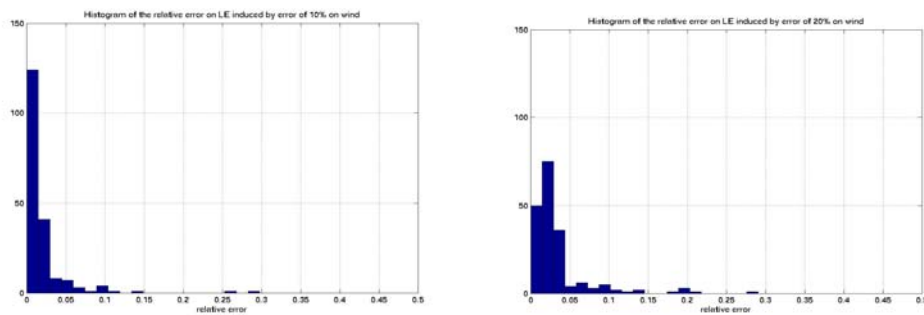
Figure 13 Distribution of the relative error induced by uncertainty on wind, of 10% on the left and of 20% on the right.

From Figure 12, we conclude that induced error of less than 10% occurs if DSSF is greater than 300 W/m², 500 W/m² and 400 W/m², for individual sensitivity analyses 1,2 and 3 respectively. Figure 13 shows that uncertainty of 10% or 20% on wind speed induces relative error less than 5% on ET.

The global error on ET estimation induced by uncertainties on radiation terms and meteorological variables considered together are shown in Figure 14 and Figure 15. As for individual sensitivity tests, we display in figure 14 ET induced uncertainty as a function of short-wave incoming radiation measured at the surface.
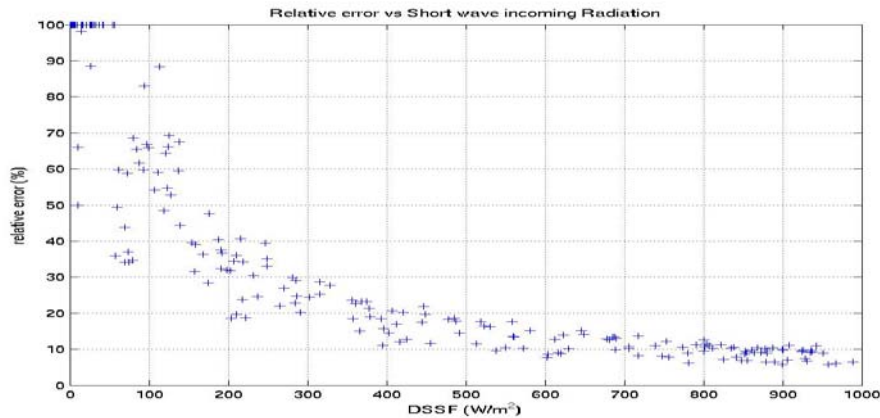
Figure 14: Dependence of the relative error induced by uncertainty on wind, air temperature, specific humidity, albedo, DSSF and DSLF on DSSF.
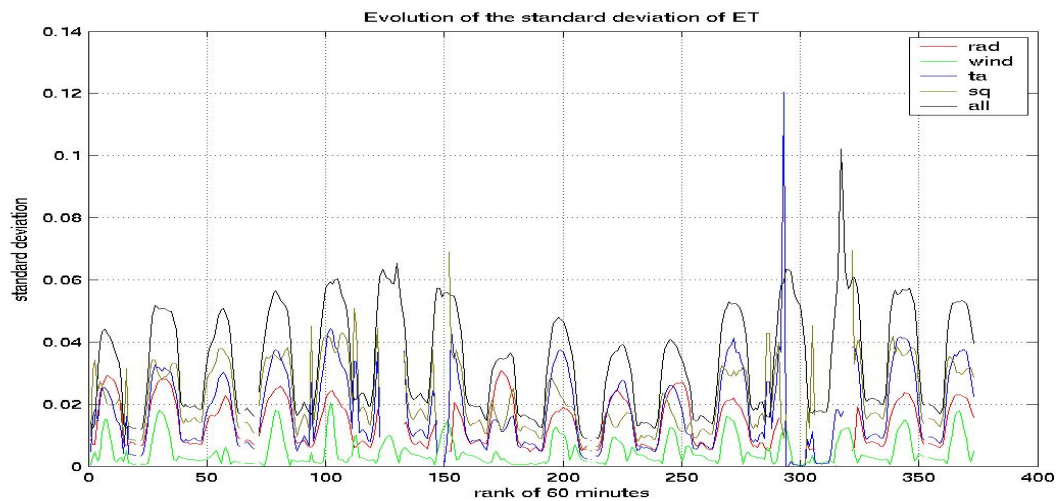
Figure 15: Superposition of the individual errors (colour lines) and of the overall error evaluated (black line). Comparing individual errors, we conclude that the major sensitivities come from air specific humidity and air temperature. The positive conclusion is that the overall error is less than the sum of the individual errors.

As a conclusion of this last test, we can quantify the contribution of each variable to the overall error by comparing results from individual sensitivity tests, as seen in Figure 15. The graph shows that the combined sensitivity analysis gives an overall uncertainty lower than the sum of individual uncertainties. This point was also noted by Gellens-Meulenberghs (2005) with a different sensitivity study. Based on the adopted uncertainties, ET algorithm is more sensitive to radiation than to wind speed. Sensitivity to air temperature and specific humidity seems also very important.

From Figure 14 and 15, we can note that uncertainty in ET shows a diurnal cycle, with a relative error less than 25% of the actual value (PRD quality criterion) for short-wave incoming radiation greater than 300 W/m², i.e. most of the diurnal values. For large zenithal angles, relative error is growing beyond 25%, however, absolute error becomes small, as seen in Figure 15, in agreement with the PRD quality criterion for small ET values.

5   Product description

The MET algorithm produces evapotranspiration estimates in mm/h over the full MSG disk (four LSA-SAF defined windows) at MSG/SEVIRI spatial resolution with a 30 minutes time step. Together with the ET map, a quality flag image is also generated. This image has the same size as the ET image and provides information on pixel-by-pixel basis. It informs about the quality of input variables and if pre/post-processing (gap filling) was performed on input or output data. Figures 16, 17, 18 and 19 present evapotranspiration estimates over different MSG regions and the corresponding quality flag images for the day 1st August 2007 at 12 h UTC.

Figure 16, Evapotranspiration images (on the left) over Europe and corresponding Quality flags images (on the right) for the 1st August 2007 at 3 different hours (0900, 1200 and 1500).

ET [m/h] for 20070801 at 12:00 UTC

ET quality flag 20070801 at 12:00 UTC

ET [m/h] for 20070801 at 15:00 UTC

ET quality flag 20070801 at 15:00 UTC

Figure 17, Evapotranspiration images (on the left) over North of Africa and corresponding Quality flags images (on the right) for the 1ˢᵗ August 2007 at 2 different hours (1200 and 1500).

ET [m/h] for 20070801 at 12:00 UTC

ET quality flag 20070801 at 12:00 UTC

ET [m/h] for 20070801 at 15:00 UTC

ET quality flag 20070801 at 15:00 UTC

Figure 18, Evapotranspiration images (on the left) over South of Africa and corresponding Quality flags images (on the right) for the 1ˢᵗ August 2007 at 2 different hours (1200 and 1500).

ET [m/h]   for 20070801 at   12:00 UTC   ET quality flag   20070801   at 12:00 UTC

ET [m/h]   for 20070801 at   15:00 UTC   ET quality flag   20070801   at 15:00 UTC
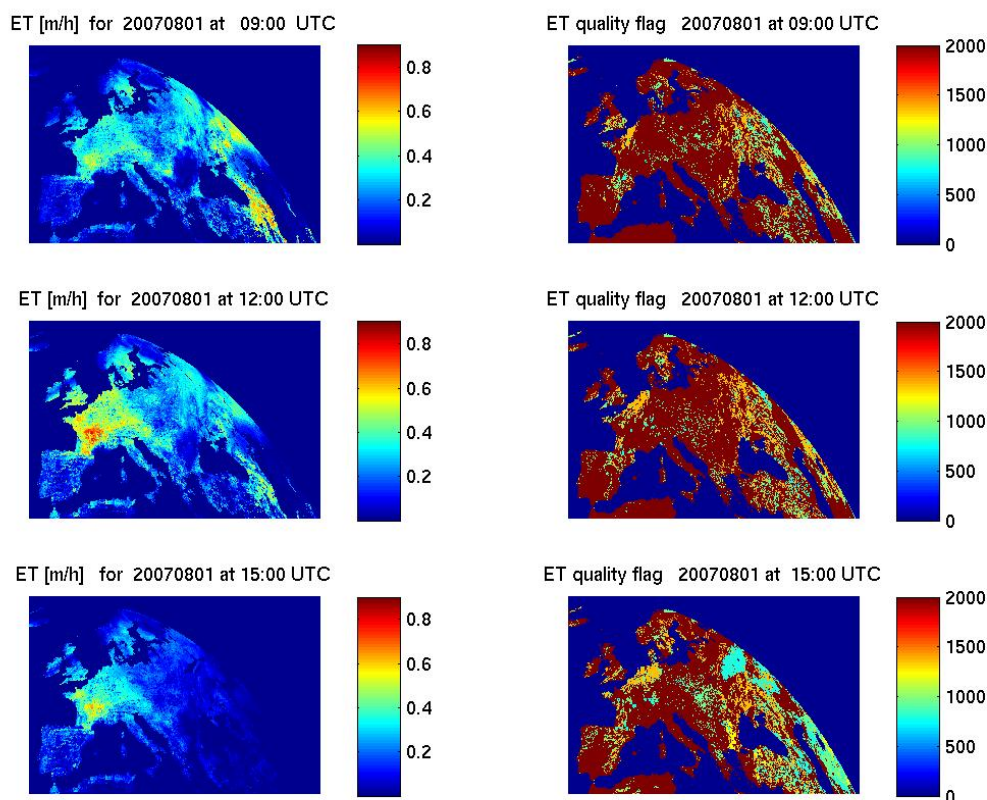
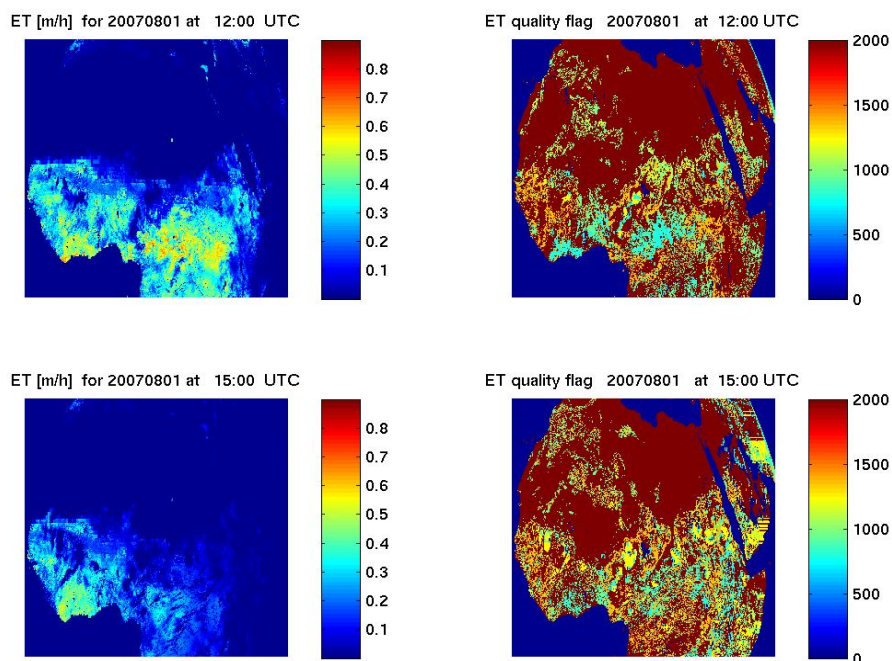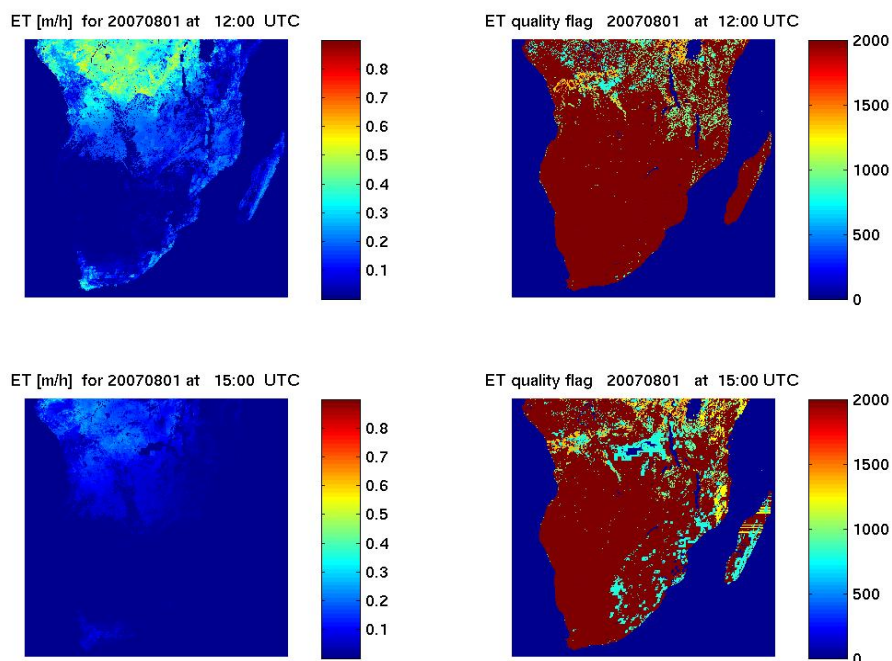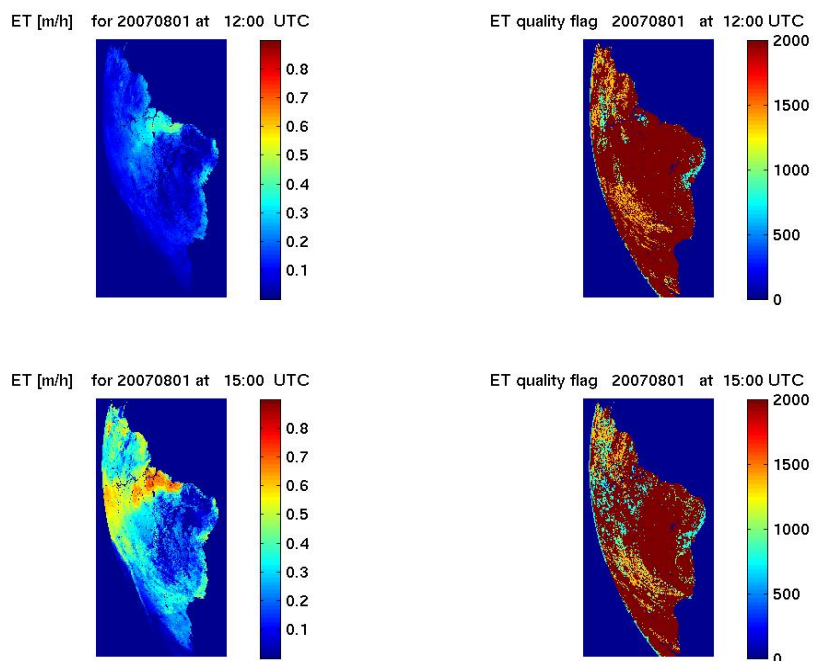*Figure 19, Evapotranspiration images (on the left) over South America and corresponding Quality flags images (on the right) for the 1ˢᵗ August 2007 at 2 different hours (1200 and 1500).*
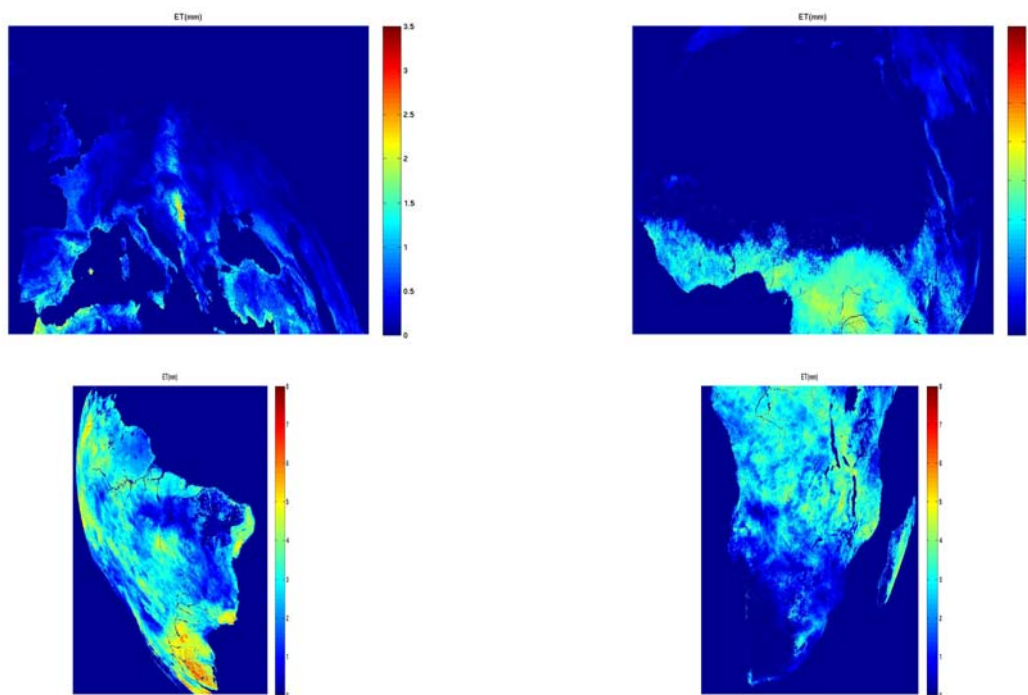
Figure 20, daily evapotranspiration (mm d⁻¹) images over Europe (upper left), North Africa (upper right), South America (bottom right) and South Africa (bottom right) for the 1ˢᵗ December 2009.

DMET product is provided with 2 images informing the number of values (slots) missing for each pixel and the percentage it represents. The Figure 20 shows an example of daily ET result.

6   Global quality and added value

Global quality
As shown in the companion 'validation report' (ET validation report 2008), the LSA-SAF ET version 04 was extensively validated over more than 20 ground reference sites over the world Results provide confidence that the LSA-SAF ET is robust and capable of reproducing ET estimates with a range of uncertainty similar to measurements uncertainty.

While the comparisons with the output from well-known models like ECMWF and GLDAS show that similar values ranges are produced, it doesn't provide conclusions about the quality of the product. It allows nevertheless detecting some areas where largest discrepancies occur what can be very useful to focus attention and check if modeling improvements are needed.

Based on the current results, we conclude that the performances of the algorithm are in general very good.

Added value
The LSA-SAF ET approach has the following advantages:

1) compared to the results of empirical approaches, the applicability of LSA-SAF ET methodology is not restricted to a few particular areas with same characteristics as used for calibration sites, but is possible over large areas;

2) compared to most remote sensing approaches, LSA-SAF ET results are provided for all nebulosity conditions (clear sky, cloudy, overcast situations); short time step results can be integrated to provide meaningful sums of actual ET over longer time steps;

3) compared to results deduced from polar satellites, LSA-SAF ET results are provided with a higher frequency (30 minutes) allowing to monitor the ET diurnal cycle and quickly evolving fluctuations associated to cloud cover variations at short time step;

4) compared to results deduced from polar satellites, daily total values, or multiple days sums, are readily obtained by adding the contribution of each 30 minutes time steps; no assumption about a constant evaporation fraction through the days is needed to compute LSA-SAF ET, neither at short time step, nor over longer periods;

5) compared to ET output from NWP models, dependency of forecast errors is limited by the use of forcing derived from remote sensing; in particular, clouds location is accurately monitored (not predicted) which allows to better estimate surface radiative fluxes used as mains drivers to compute LSA-SAF ET;

6) compared to ET output from GCMs and GLDAS, LSA-SAF ET is available for users with a higher temporal (30 minutes) and spatial resolution (MSG spatial resolution);

7) compared to ET output from LAMs, LSA-SAF ET is produced with a uniform methodology over a considerably larger spatial domain (MSG full disk);

8) thanks to the collaboration of a large panel of flux providers, LSA-SAF ET is extensively validated (see Validation Report) and submitted to a continuous validation process aiming to increase reference series length and the number of validation sites; validation is done both over past fields campaigns and with flux data coming from operational measurements networks; validation strategy includes both local and regional spatial scales and can be considered at the top of what is currently available in the scientific litterature;

9) based on the validation activity results, research is continuously pursued in view to improve LSA-SAF ET methodology.

One important advantage of the ET algorithm is its capability of generating ET estimates in all weather conditions. This characteristic will be appreciated by researchers involved in hydrological modeling specially those dealing with models with time-steps less than one day. The ET product could also interest people involved in agriculture and water management since ET can be used as an indicator of the water shortage. Spatial resolution is also an advantage for users involved in environment monitoring and climate survey. For people dealing with NWP, the ET product needs to be based on additional SRS input. Research will be pursued in this direction in the future.

7   References

Bastiaassen, W.G.M. 1995. Regionalization of surface flux densities and moisture indicators in composite terrain. Ph.D. thesis, SC-DLO, Wageningen, The Netherlands. 271pp.

Beljaars A.C.M., Viterbo P., 1994: The sensitivity of winter evaporation to the formulation of aerodynamic resistance in the ECMWF model, *Boundary-Layer Meteorol. Vol. 71, pp. 135-149.*

Chehbouni, A., Lo Seen, D. , Njoku, E.G. and Monteny, B. 1996. A Coupled Hydrological and Ecological modeling Approach to examine the Relationship between Radiative and Aerodynamic Surface Temperature over Sparsely Vegetated Surfaces. Remote Sensing Environment.

Choudury B.J., Idso S.B., Reginato J.R., 1987: Analysis of an empirical model for soil heat flux under a growing wheat crop for estimating evaporation by an infrared-temperature based energy balance equation, *Agr. For. Meteorol., 39, pp. 283-297.*

Courault D., Seguin B. and A. Olioso, 2005: Review on estimation of evapotranspiration from remote sensing data: from empirical to numerical modelling approaches, *Irrigation and Drainage Systems Vol. 19, pp. 223-249.*

FRIEDL, M.A., 2002, Forward and inverse modeling of land surface energy balance using surface temperature measurements. Remote Sensing of Environment, 79, pp. 344–354.

Gellens-Meulenberghs F., 2005: Sensitivity Tests of an Energy Balance Model to Choice of Stability Functions and Measurement Accuracy, *Boundary Layer Meteorology, Vol 115 (3), pp. 453-471.*

Gellens-Meulenberghs, F., Arboleda, A. & Ghilain, N., 2006: Status of development of the LSA-SAF evapotranspiration product. *Proc. 2nd LSA-SAF Training Workshop, Lisbon, 8-10 March, 10 pp.*

Gellens-Meulenberghs, F., Arboleda, A. and Ghilain, N., 2007: Towards a continuous monitoring of evapotranspiration based on MSG data. *Accepted contribution to the Proc. symposium on Remote Sensing for Environmental Monitoring and Change Detection. IAHS series. IUGG, Perugia, Italy, July 2007, 7 pp.*

Jacobsen A, Hansen BU. Estimation of the soil heat flux/net radiation ratio based on spectral vegetation indexes in high-latitude Arctic areas. *Int J Remote Sensing.* 1999;**20**:445–461.

Kustas, W. P., C. S. T. Daughtry, and P. J. Van Oevelen, 1993: Analytical treatment of the relationships between soil heat flux/net radiation ratio and vegetation indices. *Remote Sens. Environ.*, **46,** 319-330.

Masson, V., Champeaux, J. L., Chauvin, F., Meriguet, Ch. and Lacaze, R. A., 2003. Global Database of Land Surface Parameters at 1-km Resolution in Meteorological and Climate Models. *J. Climate **16**(9), 1261-1282.*

Norman J.M., Kustas W.P., Humes K.S., 1995: A two-source approach for estimating soil and vegetation energy fluxes from observations of directional radiometric surface temperature, Agr. For. Meteorol., 77, pp. 263-293.

Rodell M., P. R. Houser, U. Jambor, J. Gottschalck, K. Mitchell, C.-J. Meng, K. Arsenault, B. Cosgrove, J. Radakovich, M. Bosilovich, J. K. Entin, J. P. Walker, D. Lohmann, and D. Toll, The Global Land Data Assimilation System, 2004a: *Bull. Amer. Meteor. Soc. Vol. 85(3).*

Santanello and Friedl, 2003: Diurnal covariation in soil heat flux and net radiation, *J. Appl. Meteorol., 42, pp. 851-862*.

Van den Hurk, B., Viterbo, P., Beljaars, A. and Betts, A., 2000. Offline validation of the ERA40 surface scheme. *ECMWF Techn. Memorandum No.295, 42 pp.*

Viterbo, P. and Beljaars, A., 1995. An improved surface parameterization scheme in the ECMWF model and its validation. *J. Climate **8**, 2716-2748.*

8   Developers

The development and implementation of the method is carried out by the Royal Meteorological Institute of Belgium (RMI)

Coordinator: Françoise Gellens-Meulenberghs

Developers: Alirio Arboleda
                      Nicolas Ghilain

ANNEX A: Impact of the change from Tessel to H-Tessel soil moisture into LSA-SAF evapotranspiration.

Introduction

Since November 2007, ECMWF has adopted a new parameterization for its Soil-Vegetation-Atmosphere Transfer (SVAT) scheme. The SVAT scheme named 'H-Tessel' (Balsamo et al., 2008) is now used instead of the former 'Tessel' (van den Hurk et al., 2000). One of the changes comes from the different parameterizations used that refer now to 6 different soil textures instead of a unique averaged soil type. Impacts on results are expected for any application using ECMWF soil moisture (SM) as input. Users of the previous "old" scheme SM, who will pursuing their results production in a homogeneous way, need to retrieve at first SM values compatible with the former Tessel scheme, "old" scheme SM values being re-calculated from current SM. A note has been released by ECMWF for this purpose (see http://www.ecmwf.int/products/changes/soil_hydrology_cy32r3/index.html).

The LSA-SAF MET algorithm (e.g. version v04) uses as SM input ECMWF SWVL (soil water content) for the 4 soil layers. It is anticipated that without any recalibration, the simple change from Tessel SM to H-Tessel SM as input in the MET algorithm should have a large impact on ET results.

The objective of this annex is to provide an example to illustrate this impact. The 14th June 2008 at 12h TU has been selected arbitrary for this purpose.

Tessel and H-Tessel soil moisture

Contrary to previous ECMWF soil parameterization (Tessel) which uses only one uniform soil type over the whole spatial domain, the current parameterization (H-Tessel) considers 6 different soil textures derived from the FAO soil textures maps (see figure 1).
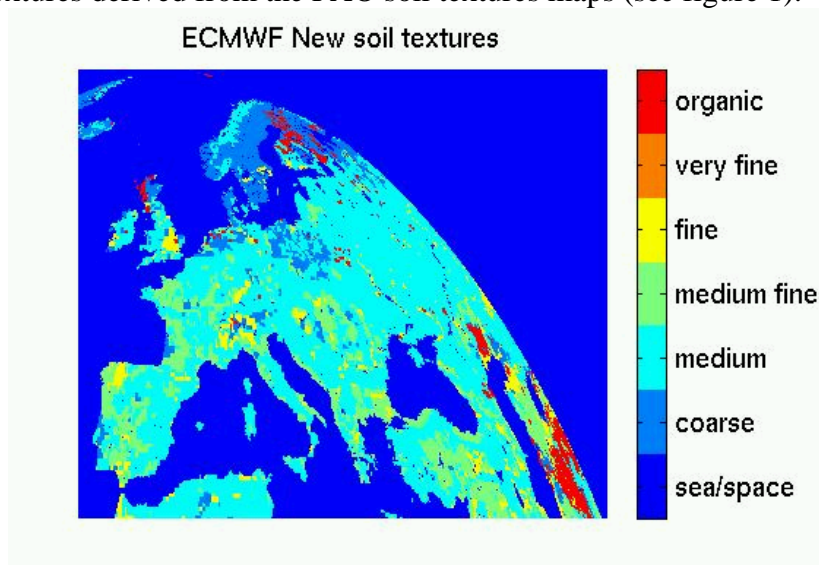

Figure 1: soil textures used by H-Tessel.

Tessel like soil moisture for the 4 soil layers have been assessed for the case of 14th June 2008 at 12h UTC from the new soil moisture following the procedure recommended by ECMWF. Figure 2 shows that SM values provided by the current parameterization in which soil texture is taken into account (left hand side) are higher than values provided by the previous parameterization where a uniform soil type was considered over the whole area (right hand side).
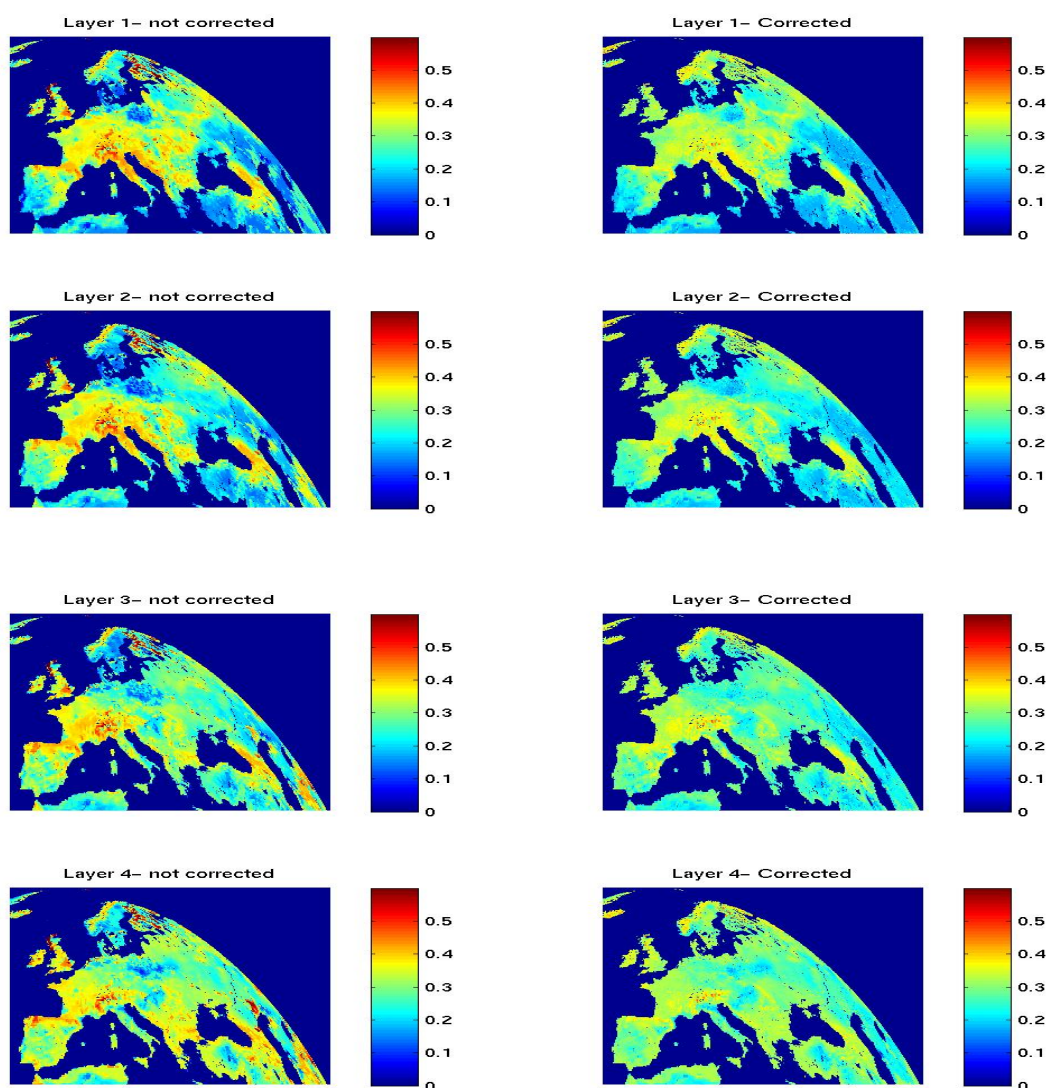

Figure 2: New H-Tessel (left) vs. old reconstructed Tessel (right) SM from ECMWF model. 14th June 2008 at 12 h UTC.

Impact on evapotranspiration

The LSA-SAF MET algorithm has been applied to compute evapotranspiration (ET) with uncorrected (H-Tessel) and corrected (rebuilt Tessel) SM, all other input data being kept unchanged (figure 3). The ET values provided with current uncorrected SM are clearly higher than ET values obtained with the old parameterization.
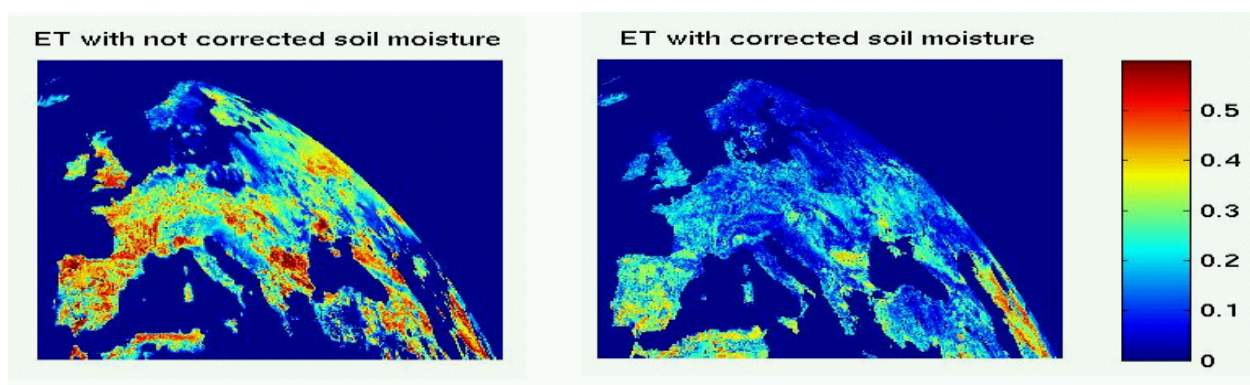
Figure 3: ET (mm.h^{-1}) computed with uncorrected (left) and corrected (right) SM input. 14th June 2008 at 12 h UTC.

Figure 4 presents a zoom from figure 3 over Belgium. On 14th June, the weather was bad over Belgium with temperatures below the normal values. Cloudiness was high with little showers.
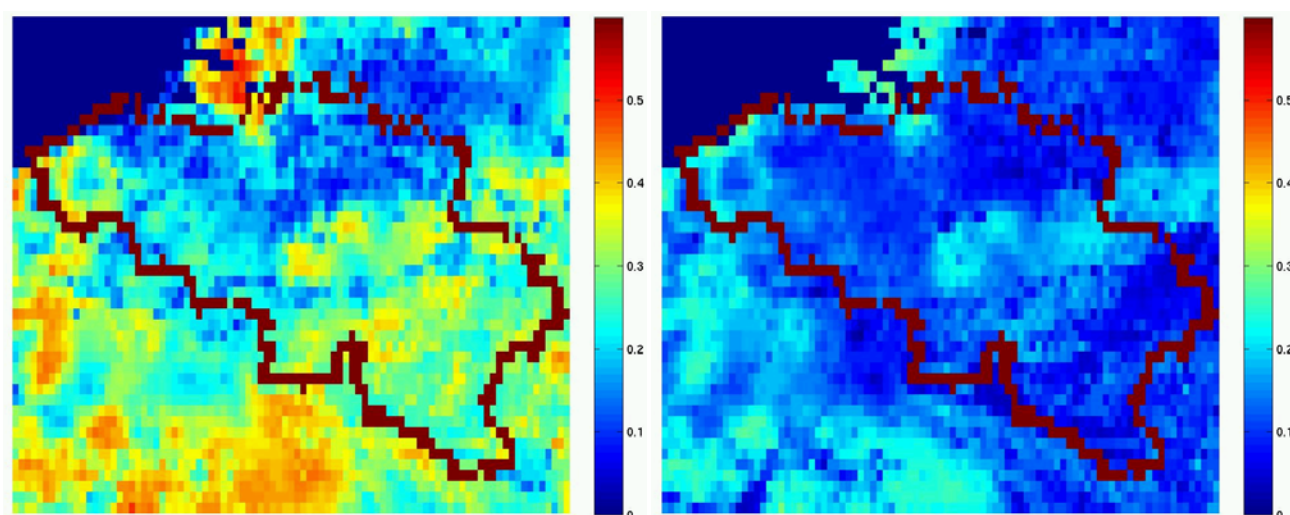

Figure 4: ET (mm.h^{-1}) over Belgium computed with uncorrected (left) and corrected (right) SM input. 14th June 2008 at 12 h UTC.

Instantaneous ET values produced by the MET algorithm with uncorrected SM ranges from 0.05 to 0.45 mm h-1 while ET values obtained with corrected SM ranges from 0.02 to 0.29 mm h-1. Mean ET values observed in 4 stations in Belgium between 11h30 and 12h30 TU were included between 0.06 and 0.25 mm h-1. Although comparisons with MET results should be done at tile level (see Validation Report) these values are more compatible with ET obtained with corrected SM values. Without any correction, ET from MET algorithm seems to be largely overestimated.

In order to provide homogeneous time series, there is a clear need to correct the new SM before using them to compute LSA-SAF ET. This insures a full compatibility with results provided in the MET v04 validation report.

Conclusion

The LSA-SAF MET algorithm has been applied to compute ET for the case of 14th June 2008 at 12h UTC. ET results obtained with uncorrected (H-Tessel) and corrected (from rebuilt Tessel) SM are completely different. It is necessary to correct the soil moisture used as input to the MET algorithm in order to produce correct ET estimates and homogeneous time series. In this way, compatibility with information provided in the Validation Report is ensured.

The correction has been implemented in the LSA-SAF operational system in July 2009. It needs to be applied in the pre-processing. Indeed, it is safer to proceed to the nomenclature change in the original ECMWF grid, before performing the spatial interpolation on the MSG grid. A clear documentation and an example of MARS script to retrieve ECMWF SWVL is provided in the note http://www.ecmwf.int/products/changes/soil_hydrology_cy32r3/index.html.

Further research is necessary in order to exploit the new ECMWF SM in the future. Recalibration of the ET algorithm will be needed. SM data from available reanalysis (ERA-40, ERA-Interim) cannot be used directly for this purpose as they are produced with the old Tessel scheme.

References

Balsamo, G., Viterbo, P., Beljaars, A., van den Hurk, B., Hirschi, M., Betts, A. K. and Scipal, K., 2008. A revised hydrology for the ECMWF model: verification from field site to terrestrial water storage and impact in the Integrated Forecast System. ECMWF Technical Memorandum N° 563, 28 pp.

van den Hurk B., Viterbo, P., Beljaars A., Betts A., 2000: Offline validation of the ERA40 surface scheme, ECMWF Technical Memorandum N° 295, 42 pp.